Identification of an Amyloid Fibril Forming Segment of Human Pmel17 Repeat Domain (RPT Domain)

Nikolaos N. Louros, Vassiliki A. Iconomidou
Department of Cell Biology and Biophysics, Faculty of Biology, University of Athens, Panepistimiopolis, Athens 157 01, Greece

Received 25 June 2015; revised 24 August 2015; accepted 18 September 2015
Published online 22 September 2015 in Wiley Online Library (wileyonlinelibrary.com). DOI 10.1002/bip.22746

ABSTRACT:

Pmel17 is the major component of functional amyloid fibrils that have an important role during pigment deposition. Pmel17 polymerization is promoted within the mildly acidic conditions of melanosomes, organelles located in pigment-specific cells. A repeat domain (RPT domain) of Pmel17, rich in glutamic acid residues has been extensively associated with the formation of the fibrous matrix. Here, we examine the RPT domain of human Pmel17 in order to provide information on this mechanism. Specifically, we have identified an aggregation-prone peptide segment (^{405}VSIVVLSGT^{413}), close to the C-terminal part of the RPT domain. Experimental results utilizing electron microscopy, X-ray fiber diffraction, Congo red staining and ATR FT-IR spectroscopy indicate that this peptide segment self-assembles forming fibrils with evident amyloidogenic properties. Conclusively, our results demonstrate that the ^{405}VSIVVLSGT^{413} peptide segment possibly has an essential role in RPT domain fibrillogenesis. © 2015 Wiley Periodicals, Inc. Biopolymers (Pept Sci) 106: 133–139, 2016.

Keywords: melanosomes; melanin; "aggregation-prone" peptide-analogue; amyloid fibrils; electron microscopy

This article was originally published online as an accepted preprint. The "Published Online" date corresponds to the preprint version. You can request a copy of any preprints from the past two calendar years by emailing the Biopolymers editorial office at biopolymers@wiley.com.

Correspondence to: Vassiliki A. Iconomidou, Department of Cell Biology and Biophysics, Faculty of Biology, University of Athens, Panepistimiopolis, Athens 157 01, Greece; e-mail: veconom@biol.uoa.gr

INTRODUCTION

The term amyloid is used to describe highly ordered fibrous protein aggregates which are impressively stable, resistant to proteases and insoluble in detergents.[1,2] Several, otherwise soluble, proteins and peptides with unrelated functions and no evident sequence or structural correlation have been associated with the formation of amyloid deposits through self-polymerizing mechanisms, which occur under certain protein-denaturing conditions.[3] Although amyloid-forming proteins do not share any similar features, amyloid fibrils are characterized by a common core, known as the cross-β fold, in which hydrogen-bonded β-strands are stacked perpendicular to the fibril axis, shaping β-sheets that are, in turn, organized parallel to the main axis of the fibril.[4,5]

Amyloid fibril formation is considered as the primary cause behind a growing number of conformational diseases, called amyloidoses, including Alzheimer's, Parkinson's, type II diabetes and several other pathological conditions.[6] Remarkably, emerging evidence has disclosed that various protective or functional fibrous protein assemblies with pivotal biological roles are based on the formation of amyloid fibrils.[7,8] Such structures, termed as functional amyloid, include, among others, protective matrices enclosing developing oocytes,[9–11] external curli fibers which are involved in the formation of Gram-negative bacteria biofilms[12] and anti-freeze proteins.[13]

A striking example of functional amyloid is the formation of the melanosome fibril arrays, which are utterly important for pigment deposition and synthesis.[14] The main component of these fibrous arrangements is a single self-aggregating protein, designated as Pmel17.[14–16] This multidomain protein comprises 668 residues, divided into nine individually folded domains.[17,18] Post-translational proteolysis of Pmel17 is

essential for the template formation, producing an N-terminal luminal part and a C-terminal fragment, termed Mα and Mβ, respectively.[16,19] Finally, proteolysis of the Mα fragment results to two additional segments, known as MαN and MαC.[20,21] The latter, includes a repeat-containing domain, designated as RPT domain which is extensively associated with the formation of the melanosomal amyloid fibril template, needed for melanin synthesis.[20,22–27] The RPT domain is composed of ten tandem imperfect 13-residue repeats, rich in proline, threonine/serine and glutamic acid (Glu) residues.[20] Extensive studies have indicated that this segment of Pmel17 has the inherent ability to self-assemble into fibrils with amyloid properties, under mildly acidic conditions (pH ~4.5-5.5).[25–27] Moreover, this process has been shown to be fully reversible, since pre-formed RPT domain fibrils dissolve once transferred into solutions with increased pH values.[26,27] This fibrillar instability has been attributed to intra/intermolecular electrostatic repulsions between the several Glu residues of the RPT domain, which are alleviated in low pH conditions.[27] Strikingly, this reversible process is essential during *in vivo* Pmel17 amyloid fibril formation, since it requires mildly acidic pH conditions, which are only found within melanosomes,[28] thus protecting from the formation of early and possibly toxic aggregates.[25] Conclusively, although another luminal domain of Pmel17, namely the polycystic kidney disease-1 like domain (PKD) has been associated with the formation of amyloid fibrils *in vitro*,[29] the reversibility of the RPT amyloid fibril formation process pinpoints this segment as the most prominent component of Pmel17 amyloid fibrils.

Accumulating biophysical and computational evidence reveals that short sequence fragments with high aggregation potential may promote the overall amyloidogenic propensity of a protein.[30,31] On this basis, we have identified a segment (encompassing residues 405-413) with high aggregation propensity, close to the C-terminal part of the RPT domain. Our experimental results, utilizing a number of biophysical techniques, including electron and polarizing microscopy, X-ray diffraction and FT-IR Spectroscopy, indicate that this peptide segment self-assembles into fibrils with distinct amyloidogenic properties. Briefly, our results provide structural insights into the formation of RPT domain amyloid fibrils by highlighting the increased amyloid-forming potency of the ^{405}VSIVVLSGT^{413} peptide segment.

MATERIALS AND METHODS

Identification of Pmel17 RPT Domain Sequence Segments With High Aggregation Propensity

The consensus tools for the prediction of sequence aggregation propensity, AMYLPRED and AMYLPRED2,[30,32] developed by our lab (available at http://biophysics.biol.uoa.gr/AMYLPRED and http://biophysics.biol.uoa.gr/AMYLPRED2), were applied on the RPT domain (residues 315-444) of human Pmel17. Consequently, a segment with high aggregation propensity, comprising residues ^{405}VSIVVLSGT^{413}, was identified (Figure 1).

Peptide Synthesis and Sample Preparation

A peptide-analogue corresponding to the aggregation-prone 405–413 region of Pmel17 was chemically synthesized. Peptide synthesis was carried out by GeneCust (Europe, Luxembourg). The peptide purity was determined to be >98% with free N- and C-terminals, respectively. The synthesized peptide was dissolved in distilled water (pH 5.35) at a concentration of 10 mg/ml. The peptide-analogue self-assembled and produced gels containing mature amyloid-like fibrils, as judged by structural work (see below), after incubation for 1-2 weeks at room temperature.

Negative Staining and Transmission Electron Microscopy

Drops (~5 μl) of the ^{405}VSIVVLSGT^{413} fibril-containing solution were applied to 400-mesh glow-discharged and carbon-coated copper grids for 60-80s. Grids were stained with a drop of 2% (w/v) aqueous uranyl acetate for 60s and the excess stain was removed by blotting with a filter paper. The grids were initially air-dried and examined with a Morgagni™ 268 transmission electron microscope, operated at 80 kV. Digital acquisitions were performed with an 11 Mpixel side-mounted Morada CCD camera (Soft Imaging System, Muenster, Germany).

X-Ray Fiber Diffraction

A droplet (5 μl) of the ^{405}VSIVVLSGT^{413} fibril-containing solution was placed between aligned capillaries with wax-covered ends (spaced 2 mm apart). The sample was air dried at ambient temperature and humidity, for 30-60 min in order to form an oriented fiber, suitable for X-ray fiber diffraction. The diffraction pattern was collected using a SuperNova-Agilent Technologies X-ray generator equipped with a 135-mm ATLAS CCD detector and a 4-circle kappa goniometer, at the Institute of Biology, Medicinal Chemistry and Biotechnology, National Hellenic Research Foundation (CuK_α high intensity X-ray micro-focus source, $\lambda = 1.5418$ Å), operated at 50kV, 0.8mA. The specimen-to-film distance was set at 52 mm. Exposure time was set to 400s. The X-ray patterns were initially viewed using the program CrysAlisPro[33] and subsequently displayed and measured with the aid of the program iMosFLM.[34]

Congo Red Staining

Suspensions of the peptide fibril-containing solution were applied to glass slides and subsequently air-dried at ambient temperature and humidity, in order to form films containing amyloid-like fibrils. The films were subsequently stained with a 1% Congo red solution in distilled water (pH 5.75) for 20 minutes, as described in previous studies.[35–38] Excess stain was removed through tap water washes. The stained films were finally observed under bright field illumination and between crossed polars, using a Leica MZ75 polarizing stereomicroscope equipped with a JVC GC-X3E camera.

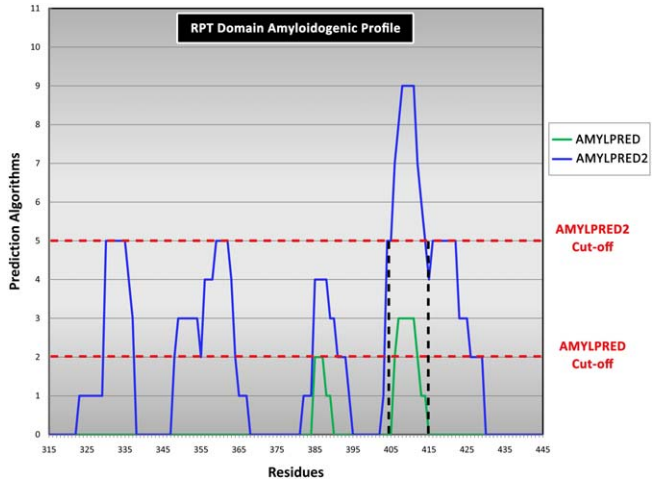

FIGURE 1 The amyloidogenic profile of the RPT domain (315-444) of Pmel17 as predicted by AMYLPRED (green line) and AMYLPRED2 (blue line). A specific region (shown by black lines), corresponding to residues ^{405}VSIVVLSGT^{413}, was predicted to have the highest aggregation potency. Both AMYLPRED and AMYLPRED2 have a default cut-off value of successful aggregation propensity prediction by at least two and five individual algorithms, respectively (shown by red lines). The horizontal axis indicates the 130 residues of the RPT domain (315-444), whereas the vertical axis corresponds to the number of individual prediction algorithms.

Attenuated Total Reflectance Fourier-Transform Infrared Spectroscopy (ATR FT-IR) Spectroscopy and Post-Run Spectra Computations

Drops (5 μl) of the ^{405}VSIVVLSGT^{413} peptide fibril-containing solution were cast on flat stainless-steel plates, coated with an ultrathin hydrophobic layer (SpectRIM, Tienta Sciences, Inc. Indianapolis, USA) and were left to air-dry slowly at ambient conditions, in order to form thin hydrated films. IR spectra were obtained at a resolution of 4 cm^{-1}, utilizing an IR microscope (IRScope II, BrukerOPTICS, Bruker Optik GmbH, Ettlingen, Germany), equipped with a Ge ATR objective lens (20×) and attached to a FT spectrometer (Equinox 55, BrukerOPTICS). Ten 32-scan spectra were collected from each sample and averaged to improve the Sound/Noise (S/N) ratio. All spectra are shown in the absorption mode after correction for the wavelength-dependence of the penetration depth (d_p analogous to λ). Absorption band maxima were determined from the minima in the second derivative of the corresponding spectra. Derivatives were computed analytically using routines of the Bruker OPUS/OS2 software, including smoothing over a $\pm$13 cm^{-1} range around each data point, performed by the Savitsky–Golay algorithm.[39] Smoothing over narrower ranges resulted in deterioration of the S/N ratio and did not increase the number of minima that could be determined with confidence. The minima in the second derivative were used to determine the corresponding absorption band maxima.

RESULTS AND DISCUSSION

A peptide segment, corresponding to residues 405–413 of the RPT domain, presenting high aggregation potential was successfully identified, by applying both algorithms developed in our laboratory, AMYLPRED and AMYLPRED2.[30,32] Specifically, the ^{405}VSIVVLSGT^{413} region is the only segment of the RPT domain that significantly overtakes the default cut-off value of both prediction tools (Figure 1). This amyloidogenic hot spot, is rich in hydrophobic residues and has a strong tendency to form β-strands, as analysis utilizing both NetCSSP[40] and SecStr[41] revealed (data not shown), both distinctive properties of amyloid-forming sequences. As a result, a peptide-analogue of this segment was studied in detail after synthesis. The ^{405}VSIVVLSGT^{413} peptide self-assembles forming thick gels containing amyloid-like fibrils, after an incubation period of 1–2 weeks. The fibrils have a uniform morphology, since they appear as thin and unbranched fibrils with a diameter of approximately 100-150 Å. Furthermore, they also exhibit a strong tendency to coalesce laterally forming wide fibril arrays of variable widths, which eventually lead to the formation of gels (Figure 2).

The X-ray diffraction pattern produced by an oriented fiber, containing more or less aligned fibrils derived by the self-assembled peptide, displays the main features of a typical "cross-β" X-ray diffraction pattern.[4] Specifically, a strong characteristic 4.7 Å reflection is seen, in addition to a 9.2 Å structural repeat, respectively (Figure 3). The former may be attributed to the periodic distance between consecutive hydrogen-bonded β-strands, which are aligned perpendicular

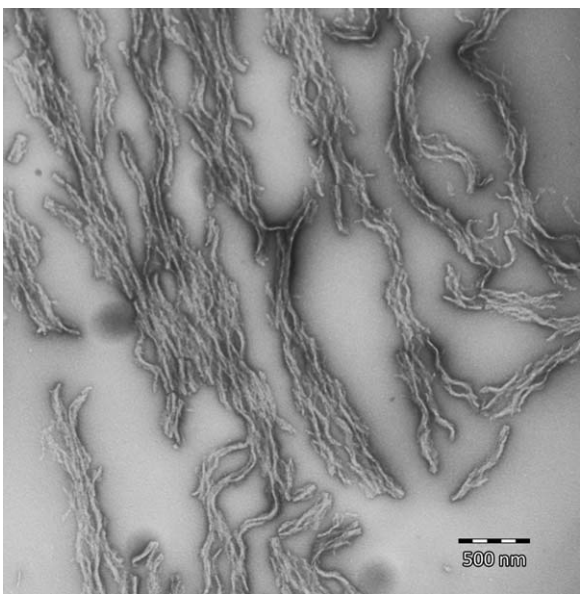

FIGURE 2 Electron micrograph indicating the aggregation propensity of the ^{405}VSIVVLSGT^{413} peptide. Amyloid fibrils formed by the self-assembling ^{405}VSIVVLSGT^{413} "aggregation-prone" peptide, appear unbranched, with a diameter of approximately 100-150 Å. Furthermore, the fibrils often interact in a lateral fashion forming ribbons of various diameters and leading to the formation of thick gels. Scale bar 500nm.

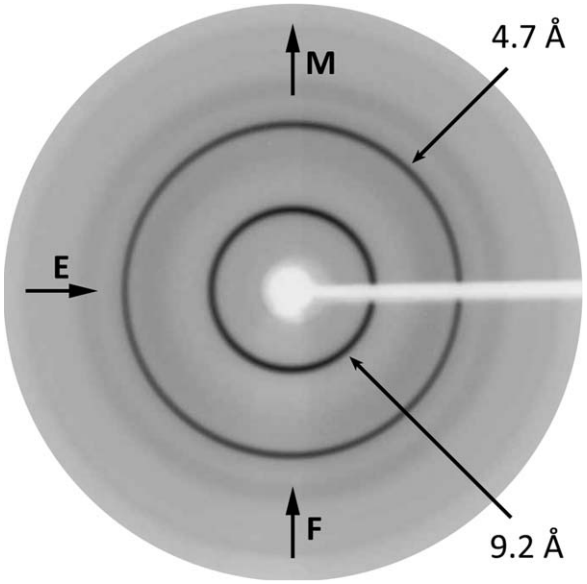

FIGURE 3 X-ray fiber diffraction pattern produced by an aligned fiber containing ^{405}VSIVVLSGT^{413} amyloid fibrils. The typical reflections of an amyloid "cross-β" pattern are displayed. The meridian (M) is vertical (direction parallel to the fiber axis, F), whereas the equator (E) is horizontal in this display. A strong 4.7 Å reflection corresponds to the repeat distance of β-strands aligned perpendicularly to the fiber axis, whereas the 9.2 Å reflection is attributed to the repetitive distance between packed β-sheets, respectively. Reflections appear as rings due to poor alignment of the oriented fiber constituent fibrils.

to the fiber axis, whereas the 9.2 Å reflection most probably arises from the repeat distance between stacked β-sheets aligned parallel to the fiber axis. Model hexapeptides corresponding to successive fragments of the VSIVVLSGT peptide were obtained scanning ZipperDB.[42] The hexapeptide coordinates are derived from threading and energetic evaluation utilizing the Rosetta-Design program. A detailed analysis of the derived hexapeptide models indicated that the accommodation of the VSIVVLSGT peptide side chains in a quarter-staggered fashion is sterically possible at a packing distance of approximately 9.2 Å, validating our experimental results. Reflections appear as rings due to poor alignment of the oriented fiber constituent fibrils.

Supporting evidence was also derived by ATR FT-IR spectral acquisitions, indicating that the amyloid-like fibrils formed, contain peptides adopting an anti-parallel β-sheet secondary structure (Figure 4). Specifically, a prominent component at 1626 cm^{-1} (Amide I) indicates the presence of a β-sheet secondary structure, supported by the 1526 and 1552 cm^{-1} components (Amide II), which are all indicative of a dominant β-sheet conformation (Table I).[43–45] Finally, an additional shoulder at 1692 cm^{-1}, implies that the β-strands may actually be aligned in an anti-parallel fashion.[43]

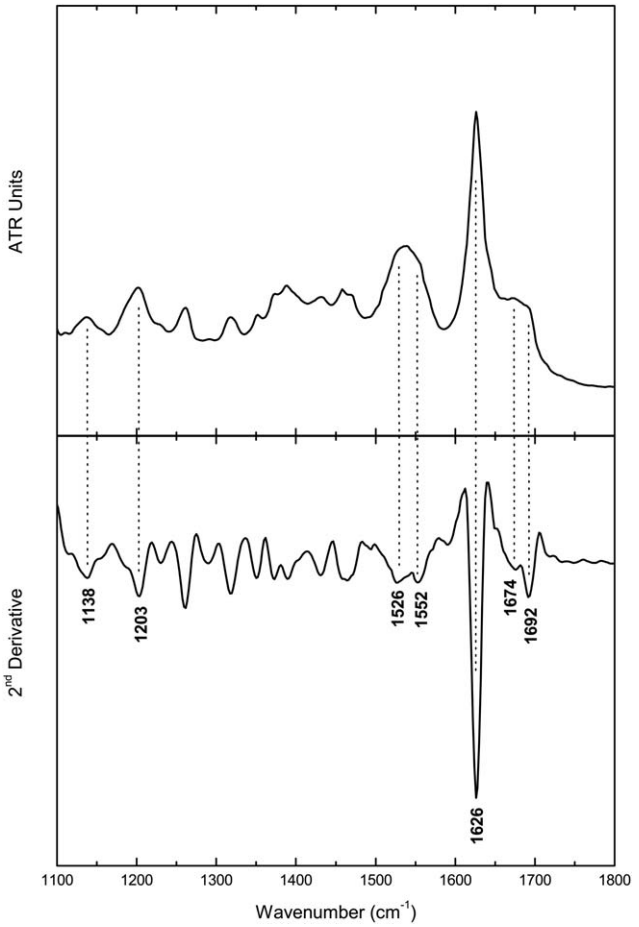

FIGURE 4 ATR FT-IR Spectrum (1100–1800 cm^{-1}) obtained from a thin hydrated film containing ^{405}VSIVVLSGT^{413} amyloid fibrils. The derived spectrum indicates that the peptide constituents of amyloid fibrils adopt an anti-parallel β-sheet secondary structure. Identification of the band maxima and their tentative assignments was performed utilizing second derivative spectral analysis (Table I).

Congo red is a stain commonly used for detection of amyloid fibrils.[46] As a result, gels containing amyloid-like fibrils formed by the ^{405}VSIVVLSGT^{413} peptide were air-dried at

Table I Bands Observed in the ATR FT-IR Spectra Produced From Hydrated Films Containing Fibrils Derived From the "Aggregation-Prone" ^{405}VSIVVLSGT^{413} Peptide, After Self-Assembly, and Their Tentative Assignments (Figure 4)

Band (cm^{-1})	Assignment
1138	TFA
1203	TFA
1526	β-sheet (Amide II)
1552	β-sheet (Amide II)
1626	β-sheet (Amide I)
1674	TFA
1692	Anti-parallel β-sheet

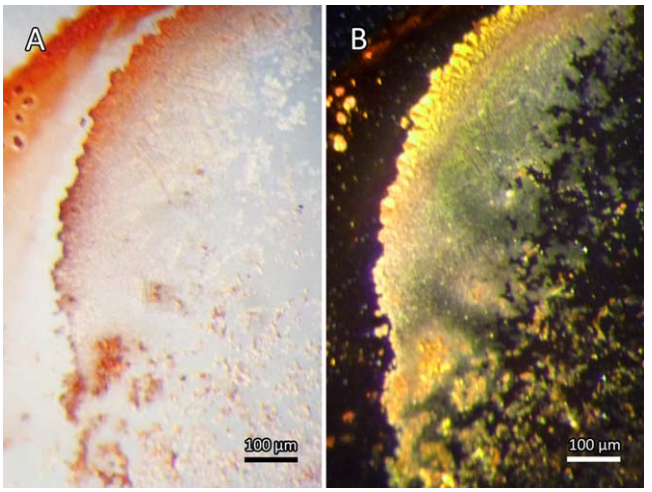

FIGURE 5 Congo red staining of ^{405}VSIVVLSGT^{413} "aggregation-prone" peptide deposits. (*A*) Gels containing amyloid fibrils formed by self-assembly of the ^{405}VSIVVLSGT^{413} peptide were positively stained with the Congo red dye, as seen under bright field illumination. (*B*) Under crossed polars, an apple/green birefringence, characteristic of amyloids, is clearly evident. Scale bars 100 μm.

room temperature in order to form films, which were subsequently stained with the Congo red dye and further observed under a polarizing microscope. Our results indicate that films containing ^{405}VSIVVLSGT^{413} amyloid-like fibrils, undoubtedly bind the amyloid-specific Congo red dye, as it is seen under bright field illumination (Figure 5A). The amyloid nature of the ^{405}VSIVVLSGT^{413} fibrils was also additionally confirmed by the characteristic apple/green birefringence, typically exhibited by Congo red stained amyloid deposits, which was clearly displayed when the stained ^{405}VSIVVLSGT^{413} films were observed under crossed polars (Figure 5B).

Clearly, the detailed experimental studies of the predicted as "aggregation-prone" ^{405}VSIVVLSGT^{413} segment of the human Pmel17 RPT domain, demonstrate that it self-assembles forming fibrillar structures presenting the basic tinctorial and structural characteristics of amyloid fibrils, validating in that manner the initial prediction of both AMYLPRED and AMYLPRED2. Remarkably, complementary evidence has derived through analysis of the RPT domain of human Pmel17 utilizing solid-state NMR.[47] During this approach, Tycko and co-workers obtained NMR spectra from three different populations of RPT domain derived amyloid fibrils. Interestingly, the aforementioned studies elucidated a notable segmental polymorphism between the different populations, since in each case different amyloid-core residue assignments emerged based on the experimental data. However, only a single RPT domain segment, encompassing residues 405-421, presented backbone assignments in all three cases. Consequently, this segment was judged to be contained within the amyloid fibril core of all three RPT populations. Our results are in agreement with the aforementioned studies, since the ^{405}VSIVVLSGT^{413} segment of the RPT domain, which was identified by our studies as an aggregation-prone interface, strongly overlaps the 405-421 segment that was highlighted as the major core segment of RPT domain derived amyloid fibrils.

The three-dimensional structure of the RPT domain of Pmel17 is currently unknown. Extensive structural and computational analysis of the RPT domain, performed by our lab, has indicated that the RPT domain of Pmel17 shares several common characteristics to β-solenoid structures (submitted manuscript). Theoretical studies have previously postulated that such β-helical domains could in fact be self-assembling components of amyloid fibrils.[48–51] This aggregation process is usually facilitated by head-to-tail interactions between exposed terminal coils, eventually leading to formation of fibrils with indeterminate length.[51,52] Impressively, a similar polymerization mechanism may occur in the case of the RPT domain of Pmel17. The identified ^{405}VSIVVLSGT^{413} aggregation-prone peptide maintains a central part of the C-terminal end of the RPT domain, extensively associated as a prime region of polymerization.[24,47] Therefore, this segment could possibly drive the RPT domain into polymerization by promoting edged H-bonding complementarity, as previously suggested for β-helical structures.[51,52] An alternative model has also been proposed, suggesting a parallel in-register arrangement for the RPT domain amyloid fibrils.[24] Following the suggested cross-β spine polymerization mechanism for amyloid,[53] suggested by the Eisenberg group, a similar mechanism may occur in the case of the RPT domain. Specifically, the intrinsic self-aggregation potency of the ^{405}VSIVVLSGT^{413} segment might separate it from the core domain to stack into a cross-β spine, with the core domain decorating the edges of the spine, in agreement to recent experimental results suggesting this segment is the main core of RPT amyloid fibrils.[47] In summary, it appears that in any case, the intrinsic self-aggregating potential of the ^{405}VSIVVLSGT^{413} segment vitally contributes in the polymerization of the RPT domain of human Pmel17.

CONCLUSIONS

Previous extensive studies have indicated that the RPT domain plays a vital role in the formation of Pmel17 amyloid fibrils. In this study, we attempt to elucidate this process. Firstly, by utilizing both aggregation propensity prediction tools, AMYLPRED and AMYLPRED2, we successfully predicted an aggregation potent segment, close to the C-terminal end of the RPT domain of human Pmel17. Finally, our experimental results, display the ability of the ^{405}VSIVVLSGT^{413} segment to

self-assemble into fibrils, presenting characteristic amyloidogenic properties, thus supporting previous studies suggesting that pinpoint residues of the C-terminal segment of RPT (overlapping the entire ^{405}VSIVVLSGT^{413} peptide) are core parts of RPT fibrils.[47] The formation of functional Pmel17 amyloid fibrils is a highly regulated and controlled process, protecting in that manner the organism from amyloid toxicity. As a result, information that could help clarify how this process is facilitated may enlighten our knowledge regarding amyloidogenesis and the differences it presents during the formation of pathological and functional amyloids.

The authors thank Prof. Stavros Hamodrakas for his unfailing interest, help and critical review. They also thank Dr. Evangelia Chrysina for help with the X-ray experiments and the Institute of Biology, Medicinal Chemistry and Biotechnology, National Hellenic Research Foundation for allowing us to use the X-ray protein crystallography facility. The help of Dr. George Baltatzis and Prof. Efstratios Patsouris and the use of the Morgagni Microscope at the 1st Department of Pathology, Medical School, University of Athens are also gratefully acknowledged. The authors sincerely thank the Editor in Chief and the Managing Editor for properly handling this manuscript and the anonymous reviewers for their very useful and constructive criticism, which helped us to considerably improve the manuscript. We also thank the University of Athens for support. The authors declare no competing financial interests.

REFERENCES

1. Dobson, C. M. Trends Biochem Sci 1999, 24, 329–332.
2. Chiti, F.; Dobson, C. M. Annu Rev Biochem 2006, 75, 333–366.
3. Fandrich, M. Cell Mol Life Sci 2007, 64, 2066–2078.
4. Sunde, M.; Serpell, L. C.; Bartlam, M.; Fraser, P. E.; Pepys, M. B.; Blake, C. C. J Mol Biol 1997, 273, 729–739.
5. Sunde, M.; Blake, C. Adv Protein Chem 1997, 50, 123–159.
6. Sipe, J. D.; Benson, M. D.; Buxbaum, J. N.; Ikeda, S.; Merlini, G.; Saraiva, M. J.; Westermark, P. Amyloid 2014, 21, 221–224.
7. Iconomidou, V. A.; Hamodrakas, S. J. Curr Protein Pept Sci 2008, 9, 291–309.
8. Maury, C. P. J Intern Med 2009, 265, 329–334.
9. Iconomidou, V. A.; Vriend, G.; Hamodrakas, S. J. FEBS Lett 2000, 479, 141–145.
10. Louros, N. N.; Iconomidou, V. A.; Giannelou, P.; Hamodrakas, S. J. PLoS One 2013, 8, e73258.
11. Louros, N. N.; Petronikolou, N.; Karamanos, T.; Cordopatis, P.; Iconomidou, V. A.; Hamodrakas, S. J. Biopolymers 2014, 102, 427–436.
12. Chapman, M. R.; Robinson, L. S.; Pinkner, J. S.; Roth, R.; Heuser, J.; Hammar, M.; Normark, S.; Hultgren, S. J. Science 2002, 295, 851–855.
13. Graether, S. P.; Slupsky, C. M.; Sykes, B. D. Biophys J 2003, 84, 552–557.
14. Fowler, D. M.; Koulov, A. V.; Alory-Jost, C.; Marks, M. S.; Balch, W. E.; Kelly, J. W. PLoS Biol 2006, 4, e6.
15. Berson, J. F.; Harper, D. C.; Tenza, D.; Raposo, G.; Marks, M. S. Mol Biol Cell 2001, 12, 3451–3464.
16. Raposo, G.; Tenza, D.; Murphy, D. M.; Berson, J. F.; Marks, M. S. J Cell Biol 2001, 152, 809–824.
17. Bailin, T.; Lee, S. T.; Spritz, R. A. J Invest Dermatol 1996, 106, 27. 2
18. Theos, A. C.; Truschel, S. T.; Raposo, G.; Marks, M. S. Pigment Cell Res 2005, 18, 322–336.
19. Berson, J. F.; Theos, A. C.; Harper, D. C.; Tenza, D.; Raposo, G.; Marks, M. S. J Cell Biol 2003, 161, 521–533.
20. Hoashi, T.; Muller, J.; Vieira, W. D.; Rouzaud, F.; Kikuchi, K.; Tamaki, K.; Hearing, V. J. J Biol Chem 2006, 281, 21198–21208.
21. Harper, D. C.; Theos, A. C.; Herman, K. E.; Tenza, D.; Raposo, G.; Marks, M. S. J Biol Chem 2008, 283, 2307–2322.
22. McGlinchey, R. P.; Shewmaker, F.; McPhie, P.; Monterroso, B.; Thurber, K.; Wickner, R. B. Proc Natl Acad Sci USA 2009, 106, 13731–13736.
23. McGlinchey, R. P.; Gruschus, J. M.; Nagy, A.; Lee, J. C. Biochemistry 2011, 50, 10567–10569.
24. McGlinchey, R. P.; Yap, T. L.; Lee, J. C. Phys Chem Chem Phys 2011, 13, 20066–20075.
25. McGlinchey, R. P.; Shewmaker, F.; Hu, K. N.; McPhie, P.; Tycko, R.; Wickner, R. B. J Biol Chem 2010, 286, 8385–8393.
26. Pfefferkorn, C. M.; McGlinchey, R. P.; Lee, J. C. Proc Natl Acad Sci USA 2010, 107, 21447–21452.
27. McGlinchey, R. P.; Jiang, Z.; Lee, J. C. Chembiochem 2014, 15, 1569–1572.
28. Bhatnagar, V.; Anjaiah, S.; Puri, N.; Darshanam, B. N.; Ramaiah, A. Arch Biochem Biophys 1993, 307, 183–192.
29. Watt, B.; van Niel, G.; Fowler, D. M.; Hurbain, I.; Luk, K. C.; Stayrook, S. E.; Lemmon, M. A.; Raposo, G.; Shorter, J.; Kelly, J. W.; Marks, M. S. J Biol Chem 2009, 284, 35543–35555.
30. Frousios, K. K.; Iconomidou, V. A.; Karletidi, C. M.; Hamodrakas, S. J. BMC Struct Biol 2009, 9, 44.
31. Lopez de la Paz, M.; Serrano, L. Proc Natl Acad Sci USA 2004, 101, 87–92.
32. Tsolis, A. C.; Papandreou, N. C.; Iconomidou, V. A.; Hamodrakas, S. J. PLoS One 2013, 8, e54175.
33. Oxford Diffraction. Chrysalis Promotions, Oxford Diffraction Ltd.: Abingdon, Oxfordshire, England, 2009.
34. Leslie, A. G. W.; Powell, H. R. Processing Diffraction Data with Mosflm, In Evolving Methods for Macromolecular Crystallography, Vol. 245; Read, R.; Sussman, J. L., Eds.; Springer: Dordrecht, The Netherlands, 2007; pp 41–51.
35. Romhanyi, G. Virchows Arch A Pathol Pathol Anat 1971, 354, 209–222.
36. Louros, N. N.; Iconomidou, V. A.; Tsiolaki, P. L.; Chrysina, E. D.; Baltatzis, G. E.; Patsouris, E. S.; Hamodrakas, S. J FEBS Lett 2013, 588, 52–57.
37. Louros, N. N.; Tsiolaki, P. L.; Zompra, A. A.; Pappa, E. V.; Magafa, V.; Pairas, G.; Cordopatis, P.; Cheimonidou, C.; Trougakos, I. P.; Iconomidou, V. A.; Hamodrakas, S. J. Biopolymers 2015, 104, 196–205.

38. Louros, N. N.; Tsiolaki, P. L.; Griffin, M. D.; Howlett, G. J.; Hamodrakas, S. J.; Iconomidou, V. A. Int J Biol Macromol 2015, 79, 711–718.
39. Savitsky, A.; Golay, M. J. E. Anal Chem 1964, 36, 1627–1639.
40. Kim, C.; Choi, J.; Lee, S. J.; Welsh, W. J.; Yoon, S. Nucleic Acids Res 2009, 37, W469–W473.
41. Hamodrakas, S. J. Comput Appl Biosci 1988, 4, 473–477.
42. Goldschmidt, L.; Teng, P. K.; Riek, R.; Eisenberg, D. Proc Natl Acad Sci USA 2010, 107, 3487–3492.
43. Surewicz, W. K.; Mantsch, H. H.; Chapman, D. Biochemistry 1993, 32, 389–394.
44. Krimm, S.; Bandekar, J. Adv Protein Chem 1986, 38, 181–364.
45. Jackson, M.; Mantsch, H. H. Crit Rev Biochem Mol Biol 1995, 30, 95–120.
46. Divry, D.; Florkin, M. Comptes Rendus De La Societe De Biologie 1927, 97, 1808–1810.
47. Hu, K. N.; McGlinchey, R. P.; Wickner, R. B.; Tycko, R. Biophys J 2011, 101, 2242–2250.
48. Lazo, N. D.; Downing, D. T. Biochemistry 1998, 37, 1731–1735.
49. Downing, D. T.; Lazo, N. D. Biochem J 1999, 343 Pt 2, 453–460.
50. Lazo, N. D.; Downing, D. T. J Pept Res 1999, 53, 633–640.
51. Kajava, A. V.; Steven, A. C. Adv Protein Chem 2006, 73, 55–96.
52. Richardson, J. S.; Richardson, D. C. Proc Natl Acad Sci USA 2002, 99, 2754–2759.
53. Nelson, R.; Eisenberg, D. Curr Opin Struct Biol 2006, 16, 260–265.